 doi:10.20944/preprints201803.0245.v1

Type of the Paper (Article)

Comparison of maximum likelihood estimators and regression models in Mediterranean forests fires for severity mapping using Landsat TM and ETM+ Data

Alexander Ariza[1,*], Javier F. Salas Rey[2] and Silvia Merino de Miguel[3]

[1] Universidad de Alcalá de Henares -UAH. Madrid – España 1; alexanderariza@edu.uah.es
[2] Universidad de Alcalá de Henares -UAH. Madrid – España 2; javier.salas@uah.es
[3] Universidad Politécnica de Madrid - UPM. Madrid – España 3; silvia.merino@upm.es
* Correspondence: alexanderariza@gmail.com; Tel.: +34-918855259

Abstract: The severity of forest fires derived from remote sensing data for research and management has become increasingly widespread in the last decade, where these data typically quantify the pre- and post-fire spectral change between satellite images on multi-spectral sensors. However, there is an active discussion about which of the main indices (dNBR, RdNBR or RBR) is the most adequate to estimate the severity of the fire, as well about the adjustment model used in the classification of severity levels. This study proposes and evaluates a new technique for mapping severity as an alternative to regression models, based on the use of the maximum likelihood estimation (MLE) automatic learning algorithm, from GeoCBI field data and spectral indices dNBR, RdNBR and RBR applied to Landsat TM, ETM+ Images, for two fires in central Spain. We compare the severity discrimination capability on dNBR, RdNBR and RBR, through a spectral separability index (M) and then evaluated the concordance of these metrics with field data based on GeoCBI measurements. Specifically, we evaluated the correspondence (R^2) between each metric and the continuous measurement of fire severity (GeoCBI) and the general precision of the regression and MLE models, for the four categorized levels of severity (Unburned, Low, Moderate, and High). The results show that the RBR has more spectral separability (average between two fires M = 2.00) that the dNBR (M = 1.82) and the RdNBR (M=1.80), additionally the GeoCBI has a better adjustment with the RBR of (R^2 = 0.73), than the RdNBR (R^2 = 0.72), and dNBR (R^2 = 0.71). Finally, the overall classification accuracy achieved with the MLE (Kappa = 0.65) has a better result than regression models (Kappa=0.58) and higher accuracy of individual classes.

Keywords: Severity mapping; Regression models; Maximum likelihood; GeoCBI; dNBR; RdNBR; RBR.

1. Introduction

Wildfire is a primary disturbance phenomenon with 200–500 million hectares being burned annually [1]. Fires affect large areas in almost all terrestrial ecosystems from tropical to boreal, being more widespread than any other natural disturbance [2,3]. In some ecosystems, e.g., savannas and grasslands, fire plays an ecologically significant role in biogeochemical cycles and disturbance dynamics, influencing the temporal variability in carbon, water, and energy fluxes. In other regions, fire may lead to the destruction of forests or to long-term site degradation. Specifically in Mediterranean countries, fire is a major hazard with an average of 45,000 fires being recorded every year, making it a substantial source of land degradation, burning an average of > 4 million hectares based on a 35-year average [4,5].

Therefore, fire constitutes one of the main factors determining the current forest landscape, these wildfires cause extensive ecological and economic losses [6] over hundreds of thousands of hectares. In Spain, although the last decade (2001–2010) has seen a reduction in the number of fire incidents (averaging 17.127 per year), the occurrence of large fires (>100 ha) has increased, in 2012, 64% of the total area affected by fires was burned in a large fire [4,7]. Even though Mediterranean species are adapted to natural fire regimes, changes in land use and the anthropogenic disturbances make vegetation communities more vulnerable to high-intensity wildfires [8]; however, these effects vary across the landscape depending on such factors as severity, intensity or recurrence of the fire[9,10].

Burn severity is a function of physical and ecological changes caused by fire, additionally, wildfires burn heterogeneously across landscapes with sections of unburned and lightly burned patches interspersed among severely burned patches, which is caused by the variability in weather, type of fire, and patch to landscape vegetation patterns. On the other hand, fire severity usually refers to changes in organic matter in stories after the wildfire. Information on burn severity and fire severity modelling is essential for land managers and ecologists who need to understand ecosystem processes especially for vegetation recovery [11], this information is also essential for emergency services for making decisions on allocating time and resources. Burn severity information is also necessary to reduce uncertainty in emission estimates [12], water quality and yield, and for the study of how burn severity affects albedo and energy partitioning [5].

Therefore, scientists and fire managers require the most accurate information available regarding the impact of fire on the environment. The key of this study, is to be able to plan better efforts for wildfire preparedness, and consequently, understand how this efforts translate to changes in actual fuel load/structure, leading this to subsequent changes in fire behavior and consequently, the fire damage potential and as well as for: vegetation recovery monitoring, wildlife studies, soil and hydrologic changes, among various ecological processes [13]. Because fire causes a number of physical changes, including consuming different layers of vegetation strata, destroying leaf chlorophyll, exposing soil, charring stems and ground, changing soil chemical composition [14] and altering both above-ground and below-ground moisture [15]; the burn severity can be related directly to the degree of this change. Such physical transformation causes variations in surface reflectance, albedo, moisture and temperature, which can be detected by means of satellite and airborne imagery [16]. Therefore, remotely sensed data can be used to measure the severity of the wildfire.

There is a wide range of remotely sensed platforms, along with applicable methods for determining the severity of a wildfire; however, the choice of approach depends on a set of particular circumstances, for instance, the conditions within the study region and the user spatial and temporal resolution needs, and the natural and climatic conditions of the study area; additionally, some sensors do not cover the required part of the electromagnetic spectrum, and vary in the number of available spectral bands. The availability of data also determines which method can be employed, such as burn algorithms, image differencing, spectral mixture analyses or fire radiative power. Within this range of remotely sensed platforms, there is a wide array of applicable methods for determining the mapping of wild land fire effects, commonly called "severity maps" [17].

Many studies have demonstrated the sensitivity of various spectral bands to significant changes in spectral radiance in burned vegetation, these spectral bands can reliably detect burnt areas, burn severity and vegetation changes. For example, near-infrared (NIR), short-wave infrared (SWIR) and thermal bands are found to be sensitive to burn magnitude changes in vegetation and are thus frequently used for fire effects studies in vegetated areas [14,18,19]. Among the most common indices for studying burn severity from satellite imagery is the NBR, which is most sensitive to changes in the vegetation. The NBR is formulated like the normalized difference vegetation index (NDVI) except for the SWIR band (2.08 um to 2.35 nm) that is used instead of the red band. The NIR wavelengths are primarily sensitive to chlorophyll, while the SWIR wavelengths are primarily sensitive to water content, ash cover, and soil mineral content [13,18].

The NBR ranges between -1 and 1 but, in common practice, NBR is scaled by 1000 to transform it to integer format [19]. The term severity involves a temporal evaluation, that is why the remotely sensed measures of severity aggregate fire effects at the time; Key and Benson used a differenced

Preprints (www.preprints.org) | NOT PEER-REVIEWED | Posted: 29 March 2018 doi:10.20944/preprints201803.0245.v1

version called dNBR, to subtract a post-fire NBR from a pre-fire NBR for mapping fires in an absolute change detection methodology, so that barren areas unchanged by fire would not appear as high severity [19]. However, one of the disadvantages of the differential indices used to map the severity is the ambiguity in the definition of the threshold of damage (Table 1), dNBR must be individually calibrated for each assessment of fire severity because of disparities in vegetation types and density [18,20].

Table 1. Variability in the definition of the thresholds of burn severity through the dNBR spectral index.

Study	Region	Severity level			
		Unburned	**Low**	**Moderate**	**High**
Parker *et al.* [21]	Australia	<77	78-257	258-427	>428
Miller and Thode [20]	California, USA	<41	41-176	177-366	>367
Key and Benson [19]	Southern Canadian	<99	100-269	270-659	>660
Hoscilo *et al.* [22]	Indonesian	<53	54-213	214-550	>550
Montealegre *et al.* [4]	Spain	<81	82-198	199-545	>545

Miller and Thode [20] present a relativized version of dNBR called RdNBR based upon adjusting in the measuring absolute change, on areas in with a sparse tree canopy. They modified dNBR by dividing by a function of the pre-fire NBR. Subsequently, Parks et al. [23] evaluate a new Landsat-based burn severity metric, the Relativized Burn Ratio (RBR), which provides an alternative to dNBR and RdNBR, improving the detection change even where pre-fire vegetation cover is low.

These spectral indices were calibrated from one-year- post-fire Landsat data to the field-collected through the Composite Burn Index (CBI), developed by Key and Benson [19] within the framework of the Fire Effects Monitoring and Inventory Protocol (FIREMON) project for pine forests in western USA, to sample these changes and to summarize the general effects of a fire at a given plot. The CBI and its modified version GeoCBI have been widely used as means for ground measurements of fire severity [24], and as an operational tool, GeoCBI visually assesses the magnitude of change by fire in five strata (soils, understory vegetation, mid-canopy, overstory, and dominant overstory vegetation) and integrates these for an overall burn severity level plot rated between zero (unburned) and three (highest severity) [19,25].

Usually, map products derived from satellite images- are produced using calibrations between the differenced spectral burn ratios (dNBR, RdNBR, RBR) to the field Burn Index (CBI, GeoCBI) percent change in tree basal area (BA), or in canopy cover (CC) [18]. None the less, it can be difficult to relate field Burn Index values to immediate fire effects [18,20,23,25], mainly because the immediate effects of fire that satellite images show, cannot always be explained through the relationship with field-based assessments of burn severity under regression models, since they also depend on factors such as ecosystem type, vegetation structure or spatial distribution among others. For this reason, the identification of complex wildfire patterns and its understanding from remotely sensed images is the key issue of burn severity mapping research programs; and in this regard, data-driven artificial intelligence and machine-learning techniques are being increasingly used to classify multispectral remotely sensed data for practical applications such as wild fire monitoring [24,26].

In this study, we propose and evaluate a new Landsat-based burn severity classification for two fires assessment, from field-based data and remotely sensed indices of burn severity for two locations in Spain, these fires did not show the same characteristics of dimension nor of damage. We developed then, a new methodological enhancement through supervised classification by maximum likelihood (MLE) for mapping burn severity, with a proposal for reducing the adjust error of traditional regression models and determine how this method impacts on classification accuracy.

The objectives of this research were to a) determine the suitability of remote sensing indices for fire severity mapping within in two different forest fires in Mediterranean ecosystems of Spain, and (b) evaluate the accuracy of supervised classification and regression models for severity mapping, derived from the differencing of pre-fire and post-fire indices from multispectral satellite data. These

Preprints (www.preprints.org) | NOT PEER-REVIEWED | Posted: 29 March 2018 doi:10.20944/preprints201803.0245.v1

objectives are conceived as developing methods for fire severity mapping by land management agencies.

2. Materials and Methods

2.1. Study Area

Our study area was located in two regions in central Spain within the grounds of the Pantano de San Juan (Madrid), and adjacent lands of Riba de Saelices Town (Guadalajara) (Fig. 1). The forest fire under study of the first area is relatively small, and it is located in south-eastern Madrid; in this case, this fire burned a total of 850 ha, with moderate to high severity, mainly composed of pine trees (*Pinus pinea*) mixed with semi- deciduous oaks and Mediterranean shrubs (*Quercus ilex)*. This region has a moderate-dry climate with evenly-distributed annual precipitation of approximately 435 mm, and an annual daily mean temperature of 13 °C [27] (Table 2).

Table 2. Summary of study areas analyzed in this study.

Region	Fire Name	Year	Field Plots	Dominance of Species	Area (ha)	Elevation (m)
Guadalajara	Riba de Saelices	2005	129	*Pino pinaster, Quercus pyrenaica, Quercus faginea*	13000	457-1328
Madrid	Pantano de San Juan	2003	61	*Pino pinea, Quercus ilex*	850	1000-1400

The second area (located in central Spain) corresponds to a large forest fire that burned 13,000 ha in 2005, mainly covered by pine forest (*Pinus pinaster*) mixed with semi-deciduous oaks (*Quercus pyrenaica* and *Quercus faginea*). A large part of this area is included in the Nature Conservancy Park (Alto Tajo), identified as a critical habitat with its core area protected. This area presents an abrupt topography, with evenly-distributed annual precipitation of approximately 650 mm, and an annual daily mean temperature of 10.2 °C [10].

Preprints (www.preprints.org) | NOT PEER-REVIEWED | Posted: 29 March 2018 doi:10.20944/preprints201803.0245.v1

Figure 1. Location of the two fires included in this study: (a) Pantano de San Juan. Madrid; (b) Riba de Saelices. Guadalajara.

2.2. *Field Data Collection*

The field-based assessment of burn severity used on both fires, was done accordingly to the standard protocol of the Geometrically structured Composite Burn Index (GeoCBI) proposed by De Santis and Chuvieco [25]. This method for estimating burn severity have into account the fraction of coverage (FCOV) of each stratum in the original CBI protocol developed by Key and Benson [19], including in the influences of overall reflectance of every plot in the calculation:

$$GeoCBI = \frac{\sum_{m_1}^{m_n}(CBI_m - FCOV_m)}{\sum_{m_1}^{m_n} FCOV_m} \quad (1)$$

where *m* refers to each vegetation stratum and *n* is the number of strata. All vegetated strata are weighed by their FCOV; the substrates stratum is not weighted. Additionally, it is included the "new sprouts" rating factor to the herbs and low shrubs stratum, including the "percent change in cover" rating factor converted to "change in leaf area index (LAI)".

The GeoCBI plot locations on the two fires were selected via stratified random sampling. Plots were stratified by burn severity, forest cover, and accessibility. GeoCBI field measurements were taken in a maximal interval of twenty-five days after the ignition date of the burnt area. The size of the plots were 30 m per 30 m, in conjunction with another studies and Landsat spatial resolution [19,28–30], the plots were located in fairly homogenous patches of a given burn severity type (90 m x 90 m). The collection of GeoCBI data was established and measured for four strata of the burn severity (unburned, low, moderate, and high), with a total of 190 plots in the two fires. On the Madrid fire, the GeoCBI was assessed with 61 plots, included ten control plots, and 103 plots on the Guadalajara fire plus 26 of control (Table 3).

Preprints (www.preprints.org) | NOT PEER-REVIEWED | Posted: 29 March 2018 doi:10.20944/preprints201803.0245.v1

Digital photos were taken from the center of each plot to the four cardinal directions to record the vegetation structure and soil condition, plus additional information. Individual coordinates of plot centers were recorded with a hand-held meter-level global positioning system (GARMIN 12 GPS), with a final accuracy of the horizontal position of sample points between an average of 5 to 15 meters.

2.3. *Remote Sensing Data*

The satellite images used in this study were acquired according to their availability and cloud coverage was Landsat 5 (TM) and Landsat 7 (ETM +) space-borne platform images. The ETM+ imagery was available prior to the wildfires on June 10, 2003, and 2005. Following the wildfires, TM imagery was acquired on July 06 and August 05, 2003, and 2005 (Table 3).

For this study, we used the standard product level L1T (Standard Terrain Correction) processing at-sensor reflectance, which was corrected to ground reflectance in order to reduce the atmospheric effects on the images. The imagery was obtained from the Glovis server of the USGS (http://earthexplorer.usgs.gov), and the ESDI (Earth Science Data Interface) server from the University of Maryland (http://glcfapp.glcf.umd.edu:8080/esdi/).

Table 3. List of imagery data used in this study.

Fire Name	Year	Landsat Path/Row	Pre-fire Imagen Date	Post-fire Imagen Date	Sensor
Riba de Saelices	2005	201/32	10/06/2003	06/07/2003	Landsat 7 ETM+ Landsat 5 TM
Pantano de San Juan	2003	200/32	10/06/2005	05/08/2005	Landsat 7 ETM+ Landsat 5 TM

2.4. Workflow

Our workflow (Figure 2) was composed of the following steps: imagery pre-processing (see Section 2.5), spectral index calculation (see Section 2.6), spectral separability analysis (see Section 2.7), burn severity classification (see Section 2.8), and accuracy assessment (see Section 2.9).

After pre-processing ETM+ and TM pre and post-fire images, multiple spectral indices were calculated. Then, the capability of the different spectral indices selected in discriminating the differences in burn severity levels was compared. Third, the adjust values of RMSE and R^2 obtained were determined in order to validate the discrimination accuracy (Section results), next, differentials images were calculated after selecting the optimal index of burn severity. Fourth, based on the targeted spectral index and GeoCBI assessment plots-field, as well as the fire perimeter, we produced a burned mask and classified burned pixels into the four burn severity levels (Unburned, Low, Moderate, and High) using two techniques: the first one, a regression model that used a field data as calibration data to estimate the burn severity; the second one, consists of a maximum likelihood estimation (MLE) approach. Finally, the overall accuracy of the burn severity map was evaluated across four affectation levels by means of a matrix error and Kappa index.

Preprints (www.preprints.org) | NOT PEER-REVIEWED | Posted: 29 March 2018 doi:10.20944/preprints201803.0245.v1

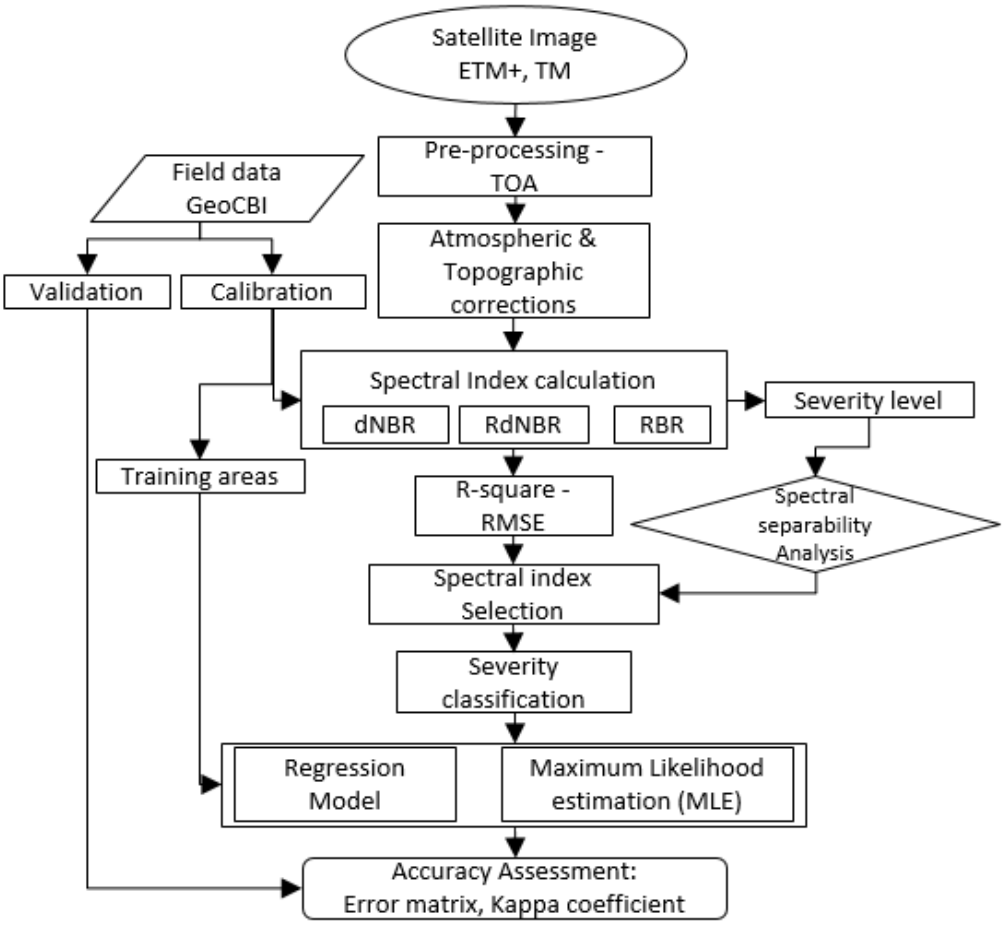

Figure 2. Flowchart of the methodology

2.5. *Imagery Pre-procesing*

Pre-processing of the remotely sensed data included geometrical rectification check, radiance conversion, subsetting, topographic and atmospheric correction.

Every multispectral band of the Landsat ETM+ and TM images were retrieved as level (L1T) data. L1T imagery had been radiometrically and sensor corrected, but without topographic and atmospheric correction replicated. As a result, all ETM+ and TM images were first ortho-rectified using the SRTM "Shuttle Radar Topography Mission" (USGS) 30 m digital elevation model (DEM) and projected to Universal Transverse Mercator coordinate system (UTM, Zone 30 North, World Geodetic System 1984).

To facilitate bi-temporal analysis, the correction accuracy of the Landsat images of 2003 and 2005 were evaluated through Root Mean Square Error (RMSE) of the metadata: 3.16 - 4.08 m, from 213 ground control points.

The atmospheric correction of satellite images is a critical step in image processing, especially when the objectives of the study are based on the analysis of spectral indices, the use of different sensors, or multitemporal analysis [13,31,32]. This correction consists of the conversion of measured radiances above the atmosphere (Top-Of-Atmosphere, -TOA-) to ground-level reflectivity (Bottom-Of-Atmosphere, -BOA-).

This study used the ATCOR atmospheric correction model included in the GEOMATICA PCI-2015 software [33]. This model calculates the reflectivity values at ground level based on the input image metadata, eliminating atmospheric effects in satellite images depending on different atmospheric conditions, aerosol types and water vapor. In addition, the spectral response of more or less illuminated areas is homogenized depending on the relief (topographic correction) and the effect of bidirectional reflectivity (BRDF) [33].

Preprints (www.preprints.org) | NOT PEER-REVIEWED | Posted: 29 March 2018 doi:10.20944/preprints201803.0245.v1

2.6. Remote Sensed Burn-Severity Indices

Many researchers consider that spectral severity indices analysis from Landsat data has shown promise for improving assessments of burn severity [24,34–36]. Most of these indices are derived from an image transformation algorithm known as the Normalized Burn Ratio (NBR), given the sensitivity of the bands of the near-infrared (NIR) and shortwave infrared (SWIR) to detect changes produced by the burn severity.

After imagery pre-processing, 6 of the most common indices used were implemented including the use of single-date and multi-date (pre- and post-burn imagery) to assess forest burn severity mapping. (Table 4).

Table 4. Spectral Indices used to classify burn severity.

Spectral index	Equation*	Reference
Normalized Difference Vegetation Index	$NDVI=(\rho NIR-\rho R)/(\rho NIR+\rho R)$	[37]
Differenced NDVI	$dNDVI= NDVI\ prefire - NDVI\ postfire$	[38,39]
Normalized Burn Ratio	$NBR = \frac{(\rho NIR - \rho SWIR)}{(\rho NIR + \rho SWIR)}$	[19]
Differenced Normalized Burn Ratio	$dNBR = NBR\ prefire - NBR\ postfire$	[19]
Relative Differenced Normalised Burn Ratio	$RdNBR = \frac{NBR\ prefire - NBR\ postfire}{\sqrt{\lvert NBR\ prefire / 1000 \rvert}}$	[20]
Relativized burn ratio	$RBR = \frac{dNBR}{(NBR_{prefire} + 1.001)}$	[23]

*R: Landsat red band; NIR: Landsat near-infrared band; SWIR: Landsat shortwave infrared band.

RdNBR and RBR have been used previously as an adjusted indices of bare ground and pre-fire vegetation during the detection of burn severity [18,20,23], we expected it could be used to improve the severity accuracy, through the adjust of the effect of the increased bare ground within the burned areas as a result of the fire-caused canopy loss.

2.7. The Separability Analysis

, The M index was calculated with the purpose of estimate the capacity of the spectral indices to differentiate the levels of fire severity identified on-field; therefore, assessing the separability of the spectral indices in discriminating burned severity effects from Landsat imagery.

A separability index (Equation (8) was used to estimate the discriminating effectiveness (i) between burned and unburned land and (ii) the spectral indices to discriminate between the different levels of burn severity. The separability index (also called normalized distance) has been used before to assess the power of mostly broadband sensors to discriminate burned areas [24,39–42]. The separability index is computed as follows:

$$M = \frac{|\mu_b - \mu_a|}{\sigma_b - \sigma_a} \quad (8)$$

where μ_b and μ_a are the mean values of the considered spectral index band of the severity levels respectively, σ_b and σ_a are the corresponding standard deviations. The separability index has been frequently used to assess the degree of discrimination in fire ecology studies for both broadband and imaging spectroscopy sensors [24,39].

Values of M index higher (M > 1) indicate good separability (better discrimination), while values lower (M < 1) represent a large degree of histogram overlap between the severity classes. Since the approach of this study is to find the best way to estimate the burn severity mapping; therefore, the sensitivity analysis was performed on the six spectral indices, based on the classification of four severity levels.

Preprints (www.preprints.org) | NOT PEER-REVIEWED | Posted: 29 March 2018 doi:10.20944/preprints201803.0245.v1

We overlaid the geo-referenced points of the different severity levels, derived from field data assessment (GeoCBI) directly on the spectral indices, and then through overload analysis extracted unburned and burned pixels of the four levels (Figure 3). During this process, field data from 153 plots was taken and employed for the study, where 61 plots corresponded to Madrid (50 GeoCBI and 11 unburned control plots) and 129 for Guadalajara (103 GeoCBI and 26 control plots).

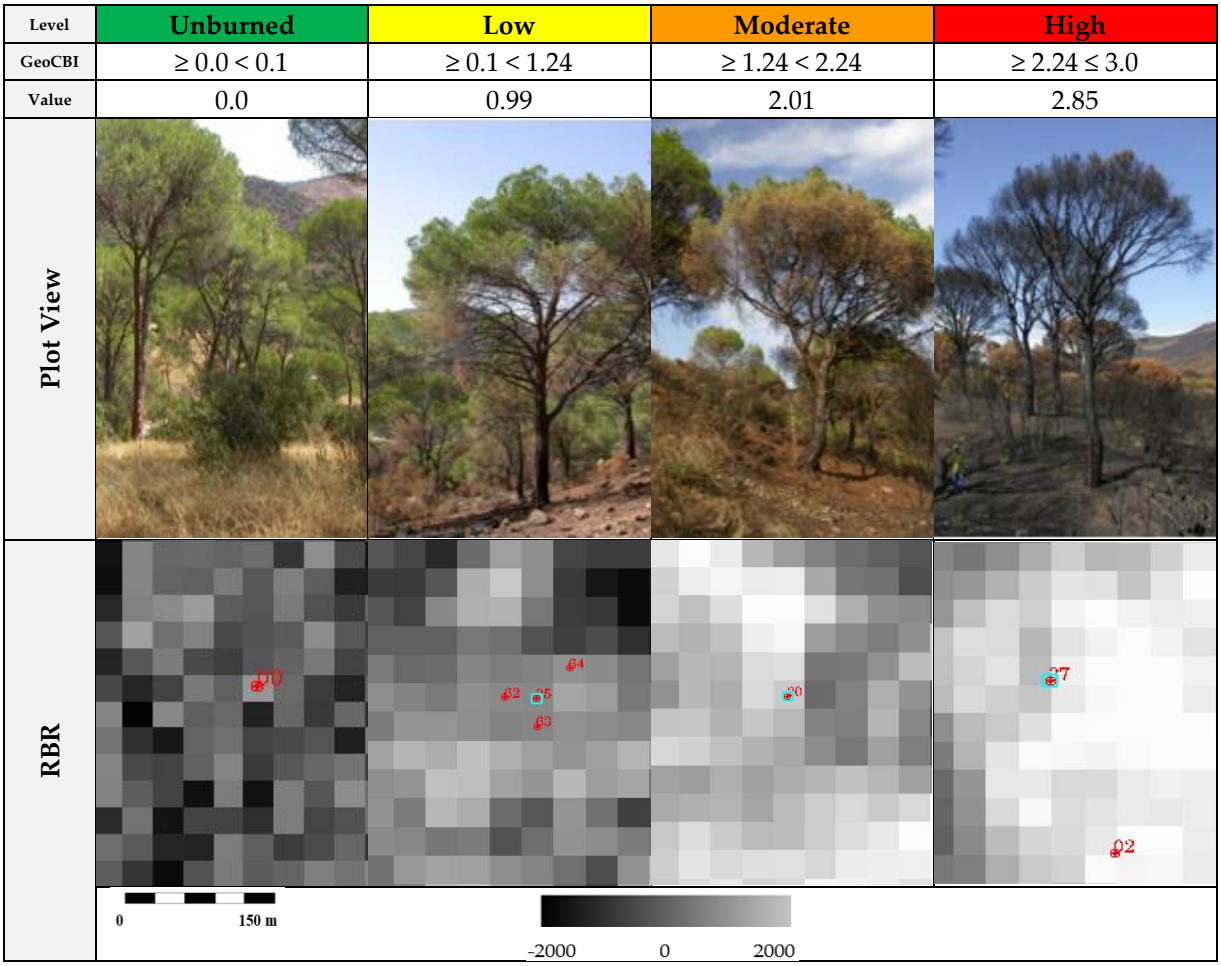

Figure 3. GeoCBI ground plots in field. The background image is the RBR spectral index in grayscale on Pantano de San Juan - Madrid.

2.8. *Burn Severity Classificaction*

The spectral index of burn severity was obtained by evaluating two parameters: (i) the spectral separability index that revealed the highest discriminatory power on the pooled dataset within each severity class, and (ii) the performance of the spectral indices (NDVI, NBR, dNDVI, dNBR, RdNBR and RBR) evaluating the correspondence of the continuous values -measured on-field GeoCBI with the coefficient of determination value R^2. Then, two classification methods were applied to map forest burn severity using both a spectral severity index and GeoCBI assessments.

The first method evaluated was based on regression models, this method evaluates the performance of the satellite-derived indices as continuous metrics of burn severity, and we tested their correspondence to GeoCBI using linear regression [18]. In previous studies, simple linear and various non-linear regression forms have been used to model the relationship between CBI or GeoCBI, and dNBR or RdNBR (e.g., [5,20,24,44]). To facilitate the comparison between our results and other studies [18,44,45], we chose to use their linear determinate by the next equation:

$$Y = a * (GeoCBI) + b \quad (9)$$

Preprints (www.preprints.org) | NOT PEER-REVIEWED | Posted: 29 March 2018 doi:10.20944/preprints201803.0245.v1

where Y is the satellite-derived metric being evaluated, a is the gain, and b is the offset value of the model. We quantified the correspondence of each metric to GoCBI as the coefficient of determination (i.e., R^2 of a linear regression between predicted and observed values) [23]. We conducted the regression for each of the 2 fires and for all 190 plots lumped together. We also conducted a validation on every plot; with 80% of the data used to train the linear model and the remaining 20% to test the model.

Next, we evaluated each remotely sensed burn severity metric's classification accuracy relative to GeoCBI. Four distinct categories (such as the defined in the study) are commonly used when mapping burn severity: unchanged (GeoCBI ≤ 0.1), low (>0.1 and ≤1.25), moderate (>1.25 and ≤2.25), and high (>2.25) [19,25]. We calculated the values of each burn severity metric that corresponded to the GeoCBI for each fire, to define the thresholds of every level using the linear regressions described in the equation (9).

The second classification method evaluated was a maximum likelihood estimation (MLE) on a spectral index image selected before (see section 2.7.), for detecting levels of ecological damage due to the burn severity. Other studies have already used supervised classifiers for mapping severity [29,46], Mitri and Gitas [47], for instance, were able to increase up to 83% overall accuracy of fire severity mapping using object-based supervised classification; in this case, we hypothesized they could improve the classification through field assessment data (GeoCBI).

Among the conventional methods of classifying multispectral imagery, such as parallelepiped, minimum distance to mean, and MLE, the latter is the most widely used algorithm for pixel-based classification, and has been shown to give the best results for classification of remotely sensed natural resource data, among the algorithms of parametric classifiers [48].

As is well known, the MLE allocates a pixel to the class with which it has the highest probability of correspondence where the likelihood $L_i(x)$ that a pixel x is a member of class (i) is given by:

$$L_i(x) = (2\pi)^{-n/2} * |V_i|^{-1/2} e^{-y/2} \quad (10)$$

where V_i is the covariance matrix of class i, n is the number of spectral bands, and y is the Mahalanobis distance. The rescaling of $L_i(x)$ between 0 and 1 yields the MLE a posteriori probability $Pi(x)$ [49].

Training sites were chosen based upon field knowledge of the four severity classes (**Figure 3**). Although is possible to generate more classes in the mapping procedure, these four were kept for training purposes due to spectral disparities between them (e.g., moderate and high). It was also important to distinguish fires from other unburned areas, so control plots outside of the perimeter were included in the training procedure.

The fire perimeters were based on remote-sensing and contrasted with the fire management office data [50], therefore, fire perimeters were created based on the remotely sensed burn-severity images, from the pre-fire NBR and the dNBR images [51,52]. Then, we applied the "burned mask" to the index-normalized images.

2.9. Accuracy Assesment

Finally, using burn severity classification maps, we evaluated classification accuracy for each fire using error matrices detailing producer's, user's, and overall accuracies and estimates of the Kappa statistic to compare the performance of the estimator MLE and regression models.

Producer's accuracy (omission error) is an evaluation of when a plot is not mapped in the correct category. User's accuracy (commission error) is an evaluation of when a plot is mapped in the wrong category. Kappa is a measure of the difference between the actual agreement between reference data and classified data, and the chance agreement between the reference data and randomly classified data.

We calculated the classification accuracy as the percentage of plots correctly classified into each burn severity class relative to field-measured GeoCBI (validation group); this was conducted for each

Preprints (www.preprints.org) | NOT PEER-REVIEWED | Posted: 29 March 2018 doi:10.20944/preprints201803.0245.v1

fire individually and all plots together. Therefore, our evaluation of best classification method involves (i) the overall classification accuracy of the fires and (ii), the classification accuracy of all severity levels analyzed; though the GeoCBI thresholds used for this classification are the most common, they are based on ecological conditions defining by the CBI and GeoCBI scale, and allow for consistent interpretation of classes across multiple fires. These GeoCBI thresholds also facilitate comparison with previous studies (e.g., [20,44]).

3. Results

3.1. Correspondence of spectral indeces to GeoCBI

In general, an analysis on the severity classes (excluding unburned) showed that the severity assessment on-field with the GeoCBI was concentrated to a greater extent on the high severity category for the two fires. In the case of Madrid, 56% correspond to High severity, followed by Moderate severity with 42%, while only 2% have Low severity. For the Guadalajara fire, High severity, typical of large Mediterranean fires, with an average GeoCBI value of 2.85, concentrated in 90.3% of the plots, 7.7% in Moderate and only 2% in Low severity (See Figure 4).

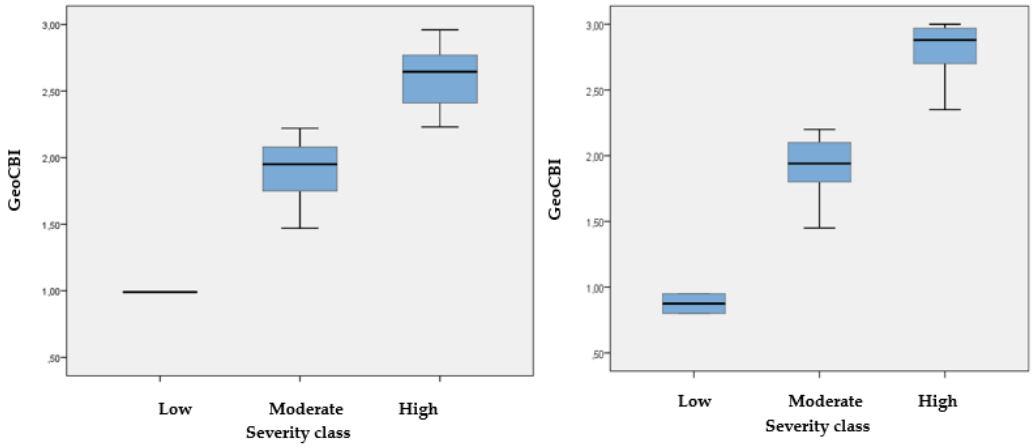

(a) (b)

Figure 4. GeoCBI distribution: (a) Boxplots in Madrid. Pantano de San Juan fire; (b) Boxplots in Guadalajara. Riba de Saelices fire; boxes represent the inter-quartile range, whiskers extend to the 5th and 95th percentiles, horizontal lines represent the median of field plots.

Regression models predicting severity (GeoCBI) based on spectral indices had a good grade of correlation R^2 and RMSE have moderate error values (Table 5), although differences between the three indices were not large.

Table 5. Variance explained and overall correlation for spectral indices, and GeoCBI.

Spectral Index	Fire name	R^2	R^2 average	R^2 adjusted	RMSE
NDVI	Riba de Saelices	0.583	0.699	0.580	0.730
	Pantano de San Juan	0.814		0.811	0.423
NBR	Riba de Saelices	0.596	0.697	0.593	0.719
	Pantano de San Juan	0.798		0.794	0.441
dNDVI	Riba de Saelices	0.615	0.694	0.612	0.702
	Pantano de San Juan	0.772		0.768	0.469
dNBR	Riba de Saelices	0.609	0.711	0.606	0.708

Preprints (www.preprints.org) | NOT PEER-REVIEWED | Posted: 29 March 2018 doi:10.20944/preprints201803.0245.v1

	Pantano de San Juan	0.812		0.809	0.408
RdNBR	Riba de Saelices	0.627		0.624	0.691
	Pantano de San Juan	0.822	0.725	0.820	0.413
RBR	Riba de Saelices	0.626		0.623	0.692
	Pantano de San Juan	0.827	0.727	0.824	0.408

Therefore, there was an indication that RdNBR and RBR consistently performed better than others. The linear regression equation we used to model the relationship between satellite-derived severity metrics and GeoCBI fit the data reasonably well (Figure 5). Averaged among two fires, the correspondence between GeoCBI and RBR was higher (R^2 = 0.727) than both RdNBR (R^2 = 0.725) and dNBR (R^2 = 0.711) (Figure 5).

(a) (b) (c)

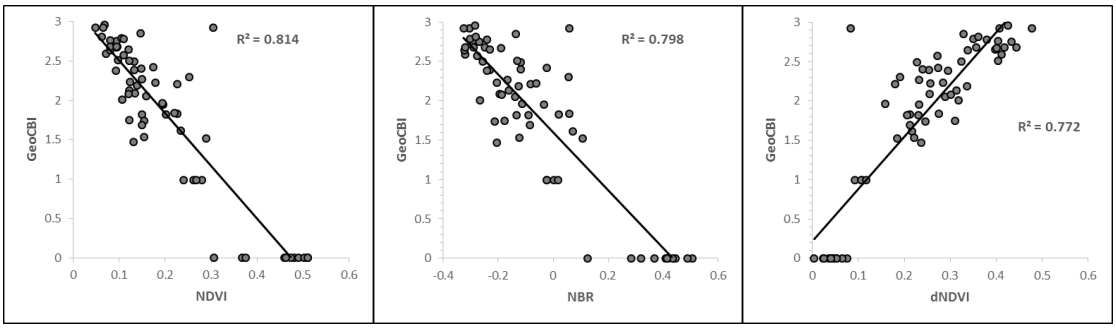

(d) (e) (f)

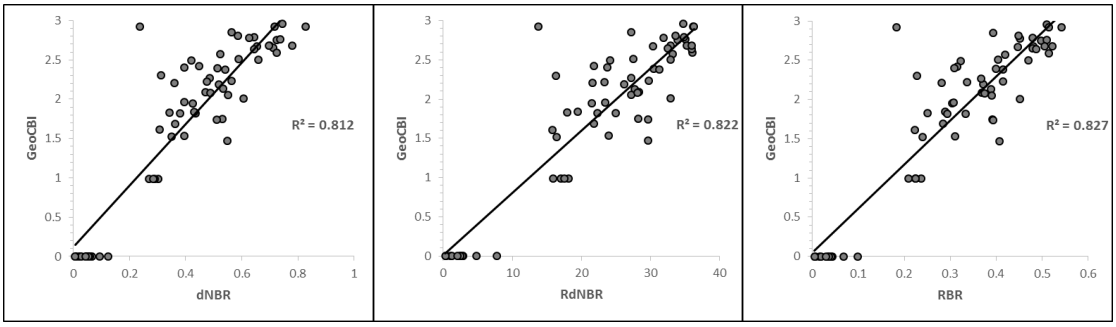

(g) (h) (i)

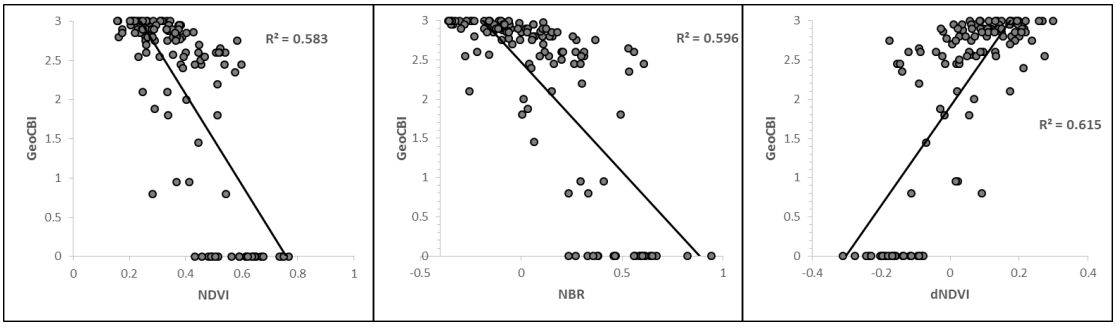

(j) (k) (l)

Preprints (www.preprints.org) | NOT PEER-REVIEWED | Posted: 29 March 2018 doi:10.20944/preprints201803.0245.v1

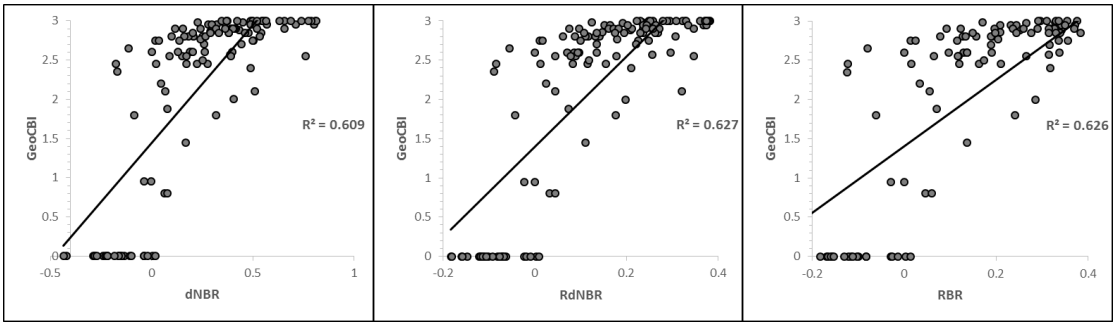

Figure 5. Scatter plots between observed burn severity GeoCBI data set (n = 190), and predicted burn severity of spectral indices. Especially in the Pantano de San Juan-Madrid fire: (a) NDVI, (b) NBR, (c) dNDVI, (d) dNBR, (e) RdNBR, and (f) RBR; from the Riba de Saelices-Guadalajara fire: (g) NDVI, (h) NBR, (i) dNDVI, (j) dNBR, (k) RdNBR, and (l) RBR.

The best adjusted R^2 values for the RBR and RdNBR models were 0.827 and 0.822 respectively, indicating better performance and highest correspondence to the GeoCBI model in explaining the variance in burn severity compared to the rest of spectral indices.

3.2. The Separability in discriminating severity levels

Figure 6 presents graphically the spectral signature plots of the burned severity on vegetation for Landsat ETM+ and TM satellite sensors, based on values extracted from sampling areas located on the satellite images. The spectral signatures of burned areas were compared for the two fires, in order to obtain a better understanding of their spectral behavior and potential discriminatory ability. It was evident that the discrimination offered by the infrared spectral channels is much higher than the visible (450 – 690 nm), despite the low spectral distance of bare land with the vegetation in the Band 4 (Near infrared: 760 – 900 nm) and the low spectral distance of bare land with the burned areas in the Band 7 Shortwave infrared, (2080 – 2350 nm). Among these, spectral Band 4 showed the highest discrimination between the severity levels and the unburned areas, followed by Band 7, Band 5, and Band 3.

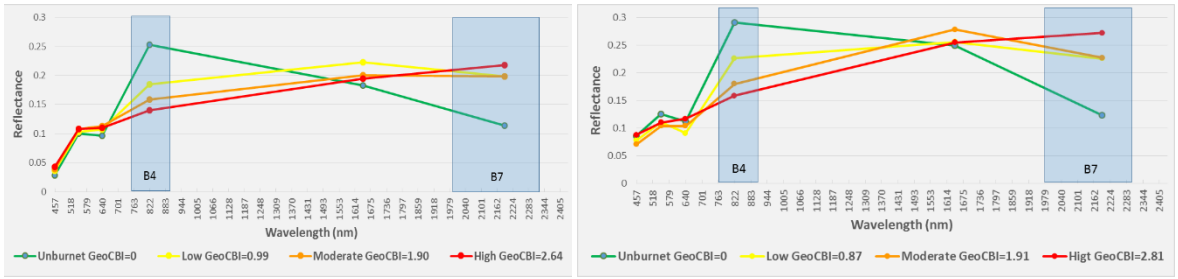

(a) (b)

Figure 2. Spectral signature of the four burned severity class on vegetation in the Landsat TM spectral channels: (a) Pantano de San Juan-Madrid fire, (b) Riba de Saelices-Guadalajara fire.

The spectral indices with the highest separability index M for each fire are listed in **Table 6**. For the pooled dataset in Madrid, the RBR spectral index had the highest M-score (M = 2.93), followed by the dNBR (M = 2.59) and RdNBR (M = 2.52) which showed moderate discriminatory power. The indices NDVI (M = 1.97), NBR (M = 1.85) and, especially, dNDVI (M = 2.36) showed very low M values. For Guadalajara fire, the RdNBR and RBR both demonstrated high discriminatory power (M=1.8 and M=1.7, respectively). The dNBR (M=1.04), the dNDVI (M=0.87), the NBR (M=0.92), and, especially, the NDVI (M = 0.70) had also very low M values.

Preprints (www.preprints.org) | NOT PEER-REVIEWED | Posted: 29 March 2018 doi:10.20944/preprints201803.0245.v1

409 **Table 6.** M index values comparing burned effects separability by level for the spectral indices.

Spectral Index	Fire name	Separability index values (M)	M average
NDVI	Riba de Saelices	0.707	1.338
	Pantano de San Juan	1.968	
NBR	Riba de Saelices	0.922	1.386
	Pantano de San Juan	1.850	
dNDVI	Riba de Saelices	0.871	1.614
	Pantano de San Juan	2.356	
dNBR	Riba de Saelices	1.040	1.815
	Pantano de San Juan	2.590	
RdNBR	Riba de Saelices	1.082	1.800
	Pantano de San Juan	2.518	
RBR	Riba de Saelices	1.068	2.000
	Pantano de San Juan	2.931	

410

411 *3.3. Spectral Index Selection*

412 In general, a high correlation is observed for all the spectral indices in both study areas. In the
413 case of Madrid, the RBR has the highest correlations with GeoCBI (R^2 = 0.827), with separability
414 values higher than (M=2.93) in the remaining indices. In the case Guadalajara, the best fit of R^2 is
415 presented for the RdNBR and RBR index (R^2=0.63), being also the two indices that presents a greater
416 separability (1.082 and 1.068) respectively.
417 According to the spectral indices correlation and discrimination results, RBR was selected for
418 subsequent forest burn severity mapping as the best index for discrimination of severity.

419 *3.4. Burn Severity Classifications*

420 Based on the previously mentioned RBR index images, the forest burn severity maps were
421 classified, first by a linear regression classification method (**Figure 7**), and second, by supervised
422 classification method "MLE".
423 We observed relatively strong correlations in the final burn severity distribution, based on the
424 regression parameters of the RBR. In the fire of Madrid, with a significant Pearson correlation of 0.897
425 and a RMSE error of 0.4398, while in Guadalajara a Pearson correlation of 0.759 and a RMSE error of
426 0.734.
427 The heterogeneity of the burned area is clearly visible, showing different severity effects in the
428 two study areas (**Figure 7**), some small unburned or low-severity patches were found to be bordered
429 by large moderate to high-severity patches; especially for Guadalajara for the high severity and
430 unburned class, where their spatial distributions were more widespread on the map.

Preprints (www.preprints.org) | NOT PEER-REVIEWED | Posted: 29 March 2018 doi:10.20944/preprints201803.0245.v1

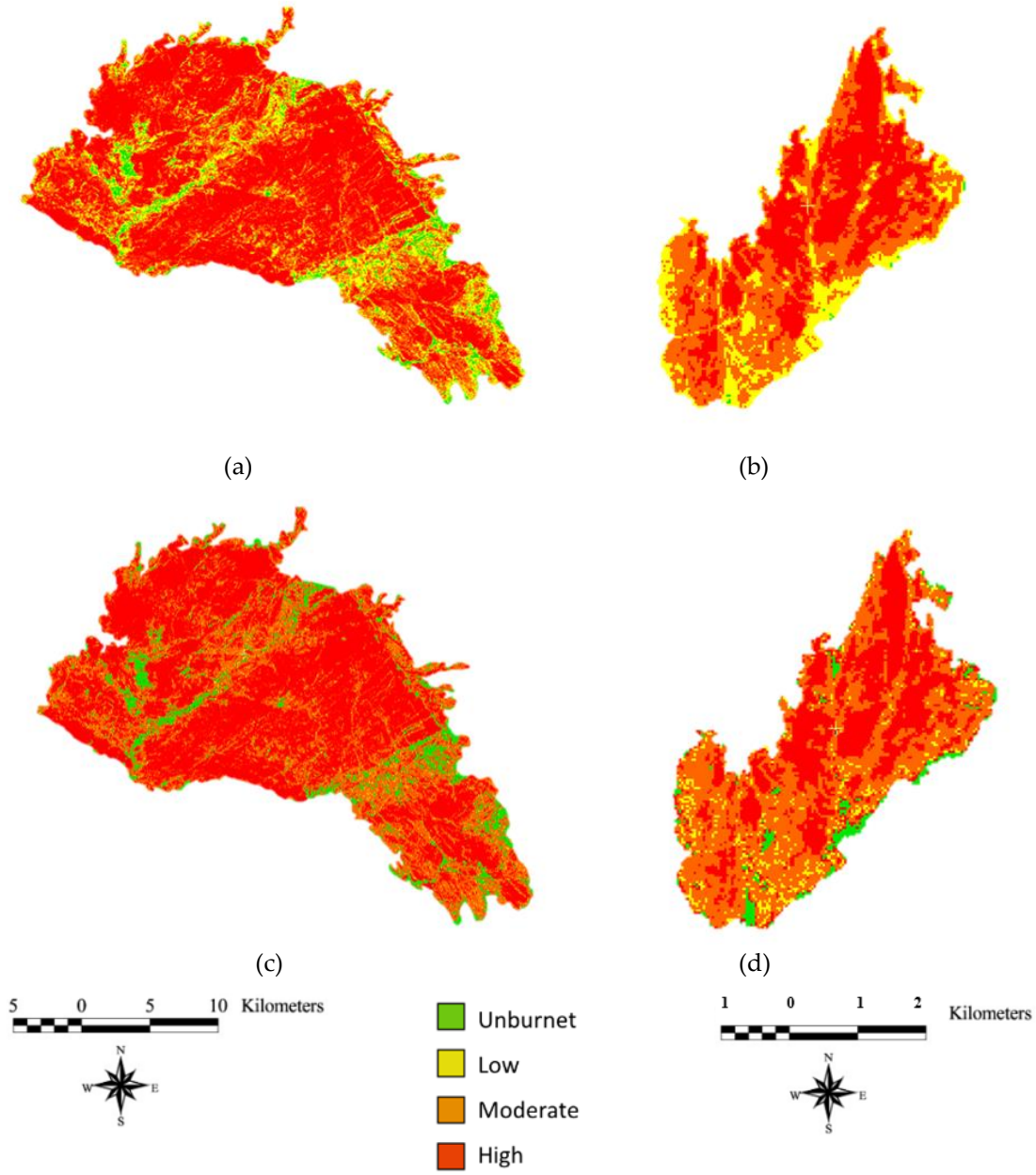

Figure 7. Spatial distributions of predicted burn severity: (a) Riba de Saelices-Guadalajara fire produced by using the linear regression; (b) Pantano de San Juan-Madrid fire by using the linear regression; (c) Riba de Saelices-Guadalajara fire produced by using the supervised classification of MLE, and (d) Pantano de San Juan-Madrid fire by the supervised classification of MLE.

On the other hand, the supervised classification with MLE was performed with the nearest neighbor as the classifier on the RBR index image, with the training samples obtained from the field survey of GeoCBI and the classification results are shown in **Figure 7**. We found that linear regression model tends to create a sub-estimate in the classification of the unburned class, and a redistribution of severity over the middle and lower classes, the upper class nevertheless continue with the same tendency.

3.5. Accuracy Assesment

Overall classification accuracies for individual fires ranged from 58% (Guadalajara) to 92% (Madrid) (**Table 7**). When averaged among fires, MLE had the highest average overall classification accuracy (75%), being greater than the linear regression model (72.5%). When all severity levels were

Preprints (www.preprints.org) | NOT PEER-REVIEWED | Posted: 29 March 2018 doi:10.20944/preprints201803.0245.v1

analyzed simultaneously, it was observed that the accuracy of classification in the lower and middle classes improved with the use of the MLE in relation to the regression model.

Classification accuracy in the moderate- and high severity classes decreased when the linear regression model, as opposed to MLE model, was used (**Table 7**). The increased classification accuracy in the moderate and low severity classes reflects differences between classification models, an effect due to the probabilistic classification of the MLE model in pixels where there is confusion between thresholds (**Figure 8**).

Table 7. Overall classification accuracy for classification models using individual burn severity classes on RBR.

Classification	Fire name	Overall accuracy	kappa	Kappa average		Classification accuracy (%)			
						Unburned	Low	Moderate	High
Regression Model	Riba de Saelices	60	0.38	0.58	User's	100	14	33	81
					Producer's	100	50	50	53
	Pantano de San Juan	85	0.77		User's	00.0	33	100	100
					Producer's	00.0	100	100	100
MLE	Riba de Saelices	58	0.41	0.65	User's	67	00.0	20	100
					Producer's	100	00.0	100	41
	Pantano de San Juan	92	0.88		User's	100	100	83	100
					Producer's	100	100	100	80

To better understand the performance of the models, we can see the frequency distributions of severity class pixels extracted from the regression model in Guadalajara represented in the Figure 8. The histograms show that burned and unburned pixels were well separated and relatively easy to discriminate, while that the frequency distribution of the severity classes (low, moderate and high) were superposed between in an upper range, compared with the frequency distribution of unburned.

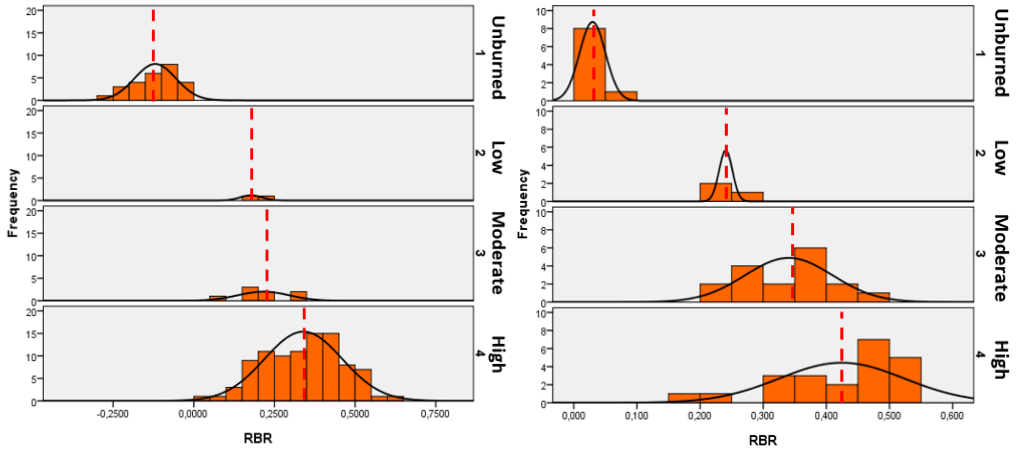

(a) (b)

Figure 8. Frequency distributions of burn severity levels extracted pixels of RBR. The vertical dash lines show a mean threshold value for discriminating burned pixels: (a) Riba de Saelices-Guadalajara; (b) Pantano de San Juan-Madrid.

 doi:10.20944/preprints201803.0245.v1

Severity class percentages were significantly different among from GeoCBI-defined field plots, but indicated a general agreement between burn severity classifications and validation field plots. Overall, the linear regression models with an average of Kappa (57.5) was mostly lower than maximum likelihood estimation model MLE (64.5).

4. Discussion

The process of burn severity mapping is critical to the understanding of the post-fire landscape change and ecosystem resilience [6,27,34,46], this has led to an increase of studies using moderate resolution satellite sensors as an approach to this issue [19,25,28]. The increased availability of moderate resolution (e.g. Landsat or Sentinel series) imagery, provides an important opportunity to map burn severity and research post-fire succession effects, making them an important resource for management activities [4,13,19,25,52]. In this study, we explored the differences in the use of supervised classification though MLE, and regression models for burn severity mapping for the first time using remotely sensed spectral indices imagery from Landsat data in a Mediterranean ecosystem.

It is important to note that it is clear that mapping burn severity at moderate spatial scales of the Landsat ETM + and TM satellite measurements, was consistent with the GeoCBI field measurements. We have observed that the results of GeoCBI in the prediction of the burn rates of remote sensing, with respect to the classification accuracy were satisfactory. In fact, the good performance of the weighted versions of the GeoCBI may be due to the fact that they emphasize the substratum and stratum, and estimate the dominant and intermediate tree strata that are more closely related to the reflectance of the plot - in their calculation [24,25,44].

The findings of our investigation can be explained, at least partially, by the spectral properties of the severity ratings of the burn according to the severity classes. Previous studies of Cansler and McKenzie [44], determined how robust spectral indices are when applied to new regions. Additionally, our study identified the spectral index that performs the best in the severity discrimination, and also the sensitivity of spectral reflectance values with respect to different levels of burn severity in areas affected by the fire.

In our study, we also assessed the separability of multiple spectral indices in discriminating burned effects in a Spain Mediterranean ecosystem. We found that spectral indices (e.g. dNBR, RdNBR), designed to account for the reflectance from the canopy affected by burn severity and proportion of pre-fire cover, tended to show higher separability (**Table 7.** Overall classification accuracy for classification models using individual burn severity classes on RBR.), like other studies on the same subject [18,20,24]. However, like the Parks *et al.* study [23], the spectral index RBR was the better corresponded to field-based burn severity measurements and had higher classification accuracy compared to dNBR and RdNBR, when discriminating different levels of severity.

These spectral indices with high discrimination power also depended on the differences between NIR, red and SWIR reflectance values. Where the effects of fire are directly related to decreasing in NIR and red spectral reflectance, as described by the studies [14,39,53].

In their study on the evaluation of spectral indices for burned area discrimination using MODIS/ASTER (MASTER) airborne simulator data Veraverbeke *et al.* [43], demonstrated that the highest sensitivity of the longer short wave infrared (SWIR) spectral region (1900–2500 nm) was observed in the interval between 2310 and 2360 nm. In our case, we observed, that the VIS (450–690 nm) regions of the indices are therefore very poor and the spectral regions of SWIR (2080–2350 nm) moderate discriminatory power, but the highest spectral separability between severity levels is observed in the spectral region of NIR (760–900 nm). This conclusion is consistent with the studies of Schepers *et al.* [39] and Arnett *et al.* [34] finding using high resolution imagery for assessing burned effects in heathlands of Europe and a mixed forest of western Canada, respectively.

User and producer specifications for moderate and low severity categories were poor for two reasons (**Table 7**): first, High, Low and Moderate categories had less than twice as many plots that others categories, it is therefore important to consider the number of plots evaluated by category, the accuracy of the register of imagery and scale of gravity maps when used for post-fire planning [18].

Second, the plot location in relation to the limit of the mapped gravity polygons is important, also plots that do not align perfectly with the 30 m satellite pixel, and how fire can move from the surface to Crown within 30 m according to Miller & Quayle [18] and Safford *et al* [54]. The fire effects can vary considerably within a pixel, this results in less precision in pixels adjacent to the edge of the polygon of wildfire, and burn severity classes.

Based on the overall accuracy of the error matrices, the approach of MLE supervised classification with an overall average accuracy of 76%, is obviously higher than the linear regression models approach, with an overall accuracy of 75%. Therefore, our evaluation of the resulting burn severity maps indicated that our MLE based approach can be used for forest burn severity mapping at moderate spatial scales from Landsat ETM + and TM data with reasonable accuracy (**Table 7**); additionally, the results were consistent across different forest fire sizes. As such, we observe that ETM+ and TM data can provide valuable information about the burned effects between severity levels.

Finally, **Figure 7** indicates that the heterogeneity of burn severity patterns was high in the two fires. Future researches could determine the relationship between the degrees of severity of the changes produced in the landscape, in order to provide information to post-fire management tasks and restoration programs, but also can provide information on changes in plant function associated with fire impacts [3,55].

5. Conclusions

Our analysis illustrates two cases in which methodological process the regression models and the maximal likelihood estimator (MLE) applied on remotely sensed indices of burn severity from Landsat imagery- in Mediterranean fires, did not show the same accuracies. We find an improved performance of MLE models over the original methods of regression for severity burn mapping, as was observed in the study areas. Nevertheless, calculation of burn severity including more categories, as well as the sensibility analysis to a larger number of ground field based (GeoCBI) training areas should be evaluated in the future. Within our study area in Mediterranean ecosystems there was a difference in the explanatory power and separability of predicting spectral indices: dNBR, RdNBR, and RBR, but the spectral index RBR may be more consistent across regions than the dNBR and RdNBR. The relationships between the geometrically structured Composite Burn Index (GeoCBI) and the RBR have about 5% more of the spectral separability and classify severity with about 10% more accurately, suggesting that the methodology is applicable and useful but could use improvement for severity mapping.

Acknowledgments: We wish to thank Angela De Santis for her help with some of the data statistics, in the same way, we also like to express our grateful thanks to the Ministries of Agriculture, Environment and Rural Development of Castilla la Mancha and the Community of Madrid, for the contribution of information for this work, and the support of the Universidad de Alcalá (UAH) and Universidad Politécnica de Madrid (UPM). Finally, we also wish to thank the anonymous reviewers whose comments greatly improved this manuscript.

Author Contributions: All co-authors of this manuscript significantly contributed to most of the phases of the investigation. A.A wrote the paper, J.S and S.M reviewed it and, A.A made the final edition and submition.

Conflicts of Interest: No potential conflict of interest was reported by the authors.

References

1. Amraoui, M.; Liberato, M. L. R.; Calado, T. J.; Dacamara, C. C.; Coelho, L. P.; Trigo, R. M.; Gouveia, C. M. Fire activity over Mediterranean Europe based on information from Meteosat-8. *For. Ecol. Manage.* **2013**, *294*, 62-75, doi:10.1016/j.foreco.2012.08.032.

2. Ichoku, C.; Giglio, L.; Wooster, M. J.; Remer, L. A. Global characterization of biomass-burning patterns using satellite measurements of fire radiative energy. *Remote Sens. Environ.* **2008**, *112*, 2950-2962, doi:10.1016/j.rse.2008.02.009.

3. Smith, A. M. S.; Sparks, A. M.; Kolden, C. A.; Abatzoglou, J. T.; Talhelm, A. F.; Johnson, D. M.; Boschetti,

L.; Lutz, J. A.; Apostol, K. G.; Yedinak, K. M.; Tinkham, W. T.; Kremens, R. J. Towards a new paradigm in fire severity research using dose-response experiments. *Int. J. Wildl. Fire* **2016**, *25*, 158-166, doi:10.1071/WF15130.

4. Montealegre, A. L.; Lamelas, M. T.; Tanase, M. A.; De la Riva, J. Forest fire severity assessment using ALS data in a mediterranean environment. *Remote Sens.* **2014**, *6*, 4240-4265, doi:10.3390/rs6054240.

5. Quintano, C.; Fernandez-Manso, A.; Roberts, D. A. Burn severity mapping from Landsat MESMA fraction images and Land Surface Temperature. *Remote Sens. Environ.* **2017**, *190*, 83-95, doi:10.1016/j.rse.2016.12.009.

6. San-Miguel-Ayanz, J.; Moreno, J. M.; Camia, A. Analysis of large fires in European Mediterranean landscapes: Lessons learned and perspectives. *For. Ecol. Manage.* **2013**, *294*, 11-22, doi:10.1016/j.foreco.2012.10.050.

7. Eleazar, M. J. .; Enríquez, E. .; Gallar, J. J. .; Jemes, V. .; López, M. .; Mateo, M. L. .; Muñoz, A. .; Parra, P. J. *Los Incendios Forestales en España, Decenio 2001–2010*; Madrid, 2013;

8. Collins, R. D.; de Neufville, R.; Claro, J.; Oliveira, T.; Pacheco, A. P. Forest fire management to avoid unintended consequences: A case study of Portugal using system dynamics. *J. Environ. Manage.* **2013**, *130*, 1-9, doi:10.1016/j.jenvman.2013.08.033.

9. Cocke, A. E.; Fulé, P. Z.; Crouse, J. E. Comparison of burn severity assessments using Differenced Normalized Burn Ratio and ground data. *Int. J. Wildl. Fire* **2005**, *14*, 189, doi:10.1071/WF04010.

10. Viedma, O.; Quesada, J.; Torres, I.; De Santis, A.; Moreno, J. M. Fire Severity in a Large Fire in a Pinus pinaster Forest is Highly Predictable from Burning Conditions, Stand Structure, and Topography. *Ecosystems* **2015**, *18*, 237-250, doi:10.1007/s10021-014-9824-y.

11. Roy, D. P.; Boschetti, L.; Trigg, S. N. Remote sensing of fire severity: Assessing the performance of the normalized burn ratio. *IEEE Geosci. Remote Sens. Lett.* **2006**, *3*, 112-116, doi:10.1109/LGRS.2005.858485.

12. Holden, Z. A.; Smith, A. M. S.; Morgan, P.; Rollins, M. G.; Gessler, P. E. Evaluation of novel thermally enhanced spectral indices for mapping fire perimeters and comparisons with fire atlas data. *Int. J. Remote Sens.* **2005**, *26*, 4801-4808, doi:10.1080/01431160500239008.

13. Chuvieco, E. *Earth observation of wildland fires in mediterranean ecosystems*; 2009; ISBN 9783642017537.

14. White, J.; Ryan, K.; Key, C.; Running, S. Remote Sensing of Forest Fire Severity and Vegetation Recovery. *Int. J. Wildl. Fire* **1996**, doi:http://dx.doi.org/10.1071/WF9960125.

15. Epting, J.; Verbyla, D.; Sorbel, B. Evaluation of remotely sensed indices for assessing burn severity in interior Alaska using Landsat TM and ETM+. *Remote Sens. Environ.* **2005**, *96*, 328-339, doi:10.1016/j.rse.2005.03.002.

16. Smith, A. M. S.; Wooster, M. J.; Drake, N. A.; Dipotso, F. M.; Falkowski, M. J.; Hudak, A. T. Testing the potential of multi-spectral remote sensing for retrospectively estimating fire severity in African Savannahs. *Remote Sens. Environ.* **2005**, *97*, 92-115, doi:10.1016/j.rse.2005.04.014.

17. Parsons, A.; Robichaud, P. R.; Lewis, S. a; Napper, C.; Clark, J. T.; Jain, T. B. Field guide for mapping post-fire soil burn severity. *Water* **2010**, 49.

18. Miller, J. D.; Quayle, B. Calibration and validation of immediate post-fire satellite-derived data to three severity metrics. *Fire Ecol.* **2015**, *11*, 12-30, doi:10.4996/fireecology.1102012.

19. Key, C. H.; Benson, N. C. *Landscape assessment (LA): Sampling and analysis methods*; 2006;

20. Miller, J. D.; Thode, A. E. Quantifying burn severity in a heterogeneous landscape with a relative version of the delta Normalized Burn Ratio (dNBR). *Remote Sens. Environ.* **2007**, *109*, 66-80,

611 doi:10.1016/j.rse.2006.12.006.

612 21. Molina, J. L.; Bromley, J.; García-Aróstegui, J. L.; Sullivan, C.; Benavente, J. Integrated water resources
613 management of overexploited hydrogeological systems using Object-Oriented Bayesian Networks.
614 *Environ. Model. Softw.* **2010**, *25*, 383-397, doi:10.1016/j.envsoft.2009.10.007.

615 22. Hoscilo, A.; Tansey, K. J.; Page, S. E. Post-fire vegetation response as a proxy to quantify the magnitude
616 of burn severity in tropical peatland. *Int. J. Remote Sens.* **2013**, *34*, 412-433,
617 doi:10.1080/01431161.2012.709328.

618 23. Parks, S. A.; Dillon, G. K.; Miller, C. A new metric for quantifying burn severity: The relativized burn
619 ratio. *Remote Sens.* **2014**, *6*, 1827-1844, doi:10.3390/rs6031827.

620 24. Meng, R.; Wu, J.; Schwager, K. L.; Zhao, F.; Dennison, P. E.; Cook, B. D.; Brewster, K.; Green, T. M.;
621 Serbin, S. P. Using high spatial resolution satellite imagery to map forest burn severity across spatial
622 scales in a Pine Barrens ecosystem. *Remote Sens. Environ.* **2017**, *191*, 95-109, doi:10.1016/j.rse.2017.01.016.

623 25. De Santis, A.; Chuvieco, E. GeoCBI: A modified version of the Composite Burn Index for the initial
624 assessment of the short-term burn severity from remotely sensed data. *Remote Sens. Environ.* **2009**, *113*,
625 554-562, doi:10.1016/j.rse.2008.10.011.

626 26. Kern, A. N.; Addison, P.; Oommen, T.; Salazar, S. E.; Coffman, R. A. Machine Learning Based Predictive
627 Modeling of Debris Flow Probability Following Wildfire in the Intermountain Western United States.
628 *Math. Geosci.* 2017, 1-19.

629 27. Ariza, A. Análisis de los cambios en la estructura del paisaje por incendios forestales mediante
630 teledetección, Alcala de Henares, 2017.

631 28. Veraverbeke, S.; Verstraeten, W. W.; Lhermitte, S.; Goossens, R. Evaluating Landsat Thematic Mapper
632 spectral indices for estimating burn severity of the 2007 Peloponnese wildfires in Greece. *Int. J. Wildl.*
633 *Fire* **2010**, *19*, 558-569, doi:10.1071/WF09069.

634 29. Henry, M. C. Comparison of Single- and Multi-date Landsat Data for Mapping Wildfire Scars in Ocala
635 National Forest , Florida. *Photogramm. Eng. Remote Sensing* **2008**, *74*, 881-891.

636 30. Arnett, J. T. T. R.; Coops, N. C.; Daniels, L. D.; Falls, R. W. Detecting forest damage after a low-severity
637 fire using remote sensing at multiple scales. *Int. J. Appl. Earth Obs. Geoinf.* **2015**, *35*, 239-246,
638 doi:10.1016/j.jag.2014.09.013.

639 31. Said, Y. A.; Petropoulos, G. P.; Srivastava, P. K. Assessing the influence of atmospheric and topographic
640 correction and inclusion of SWIR bands in burned scars detection from high-resolution EO imagery: a
641 case study using ASTER. *Nat. Hazards* **2015**, *78*, 1609-1628, doi:10.1007/s11069-015-1792-9.

642 32. Hantson, S.; Chuvieco, E. Evaluation of different topographic correction methods for landsat imagery.
643 *Int. J. Appl. Earth Obs. Geoinf.* **2011**, *13*, 691-700, doi:10.1016/j.jag.2011.05.001.

644 33. Richter, R. Atmospheric / Topographic Correction for Satellite Imagery (ATCOR - 2/3 User Guide).
645 *ATCOR-2/3 User Guid. Version 6.3* **2007**, 1-71, doi:10.1017/CBO9781107415324.004.

646 34. Arnett, J. T. T. R.; Coops, N. C.; Daniels, L. D.; Falls, R. W. Detecting forest damage after a low-severity
647 fire using remote sensing at multiple scales. *Int. J. Appl. Earth Obs. Geoinf.* **2015**, *35*, 239-246,
648 doi:10.1016/j.jag.2014.09.013.

649 35. Holden, Z. A.; Morgan, P.; Smith, A. M. S.; Vierling, L. Beyond Landsat: A comparison of four satellite
650 sensors for detecting burn severity in ponderosa pine forests of the Gila Wilderness, NM, USA. *Int. J.*
651 *Wildl. Fire* **2010**, *19*, 449-458, doi:10.1071/WF07106.

652 36. Veraverbeke, S.; Lhermitte, S.; Verstraeten, W. W.; Goossens, R. Evaluation of pre/post-fire differenced
653 spectral indices for assessing burn severity in a Mediterranean environment with Landsat Thematic

654 Mapper. *Int. J. Remote Sesning* **2011**, *32*, 3521-3537, doi:10.1080/01431161003752430.

655 37. Tucker, C. J. Red and photographic infrared linear combinations for monitoring vegetation. *Remote Sens.*
656 *Environ.* **1979**, *8*, 127-150, doi:10.1016/0034-4257(79)90013-0.

657 38. Escuin, S.; Navarro, R.; Fernández, P. Fire severity assessment by using NBR (Normalized Burn Ratio)
658 and NDVI (Normalized Difference Vegetation Index) derived from LANDSAT TM/ETM images. *Int. J.*
659 *Remote Sens.* **2008**, *29*, 1053-1073, doi:10.1080/01431160701281072.

660 39. Schepers, L.; Haest, B.; Veraverbeke, S.; Spanhove, T.; Borre, J. Vanden; Goossens, R. Burned area
661 detection and burn severity assessment of a heathland fire in belgium using airborne imaging
662 spectroscopy (APEX). *Remote Sens.* **2014**, *6*, 1803-1826, doi:10.3390/rs6031803.

663 40. Harris, S.; Veraverbeke, S.; Hook, S. Evaluating spectral indices for assessing fire severity in chaparral
664 ecosystems (Southern California) using modis/aster (MASTER) airborne simulator data. *Remote Sens.*
665 **2011**, *3*, 2403-2419, doi:10.3390/rs3112403.

666 41. Pereira, J. M.; Sa, A. C. L.; Sousa, A. M. O.; Silva, J. M. N.; Santos, T. N.; Carreiras, J. M. B. Spectral
667 characterisation and discrimination of burnt areas. *Remote Sens. Large Wildfires* **1999**, 123-138,
668 doi:10.1007/978-3-642-60164-4_7.

669 42. Pleniou, M.; Koutsias, N. Sensitivity of spectral reflectance values to different burn and vegetation ratios:
670 A multi-scale approach applied in a fire affected area. *ISPRS J. Photogramm. Remote Sens.* **2013**, *79*, 199-
671 210, doi:10.1016/j.isprsjprs.2013.02.016.

672 43. Veraverbeke, S.; Harris, S.; Hook, S. Evaluating spectral indices for burned area discrimination using
673 MODIS/ASTER (MASTER) airborne simulator data. *Remote Sens. Environ.* **2011**.

674 44. Cansler, C. A.; McKenzie, D. How robust are burn severity indices when applied in a new region?
675 Evaluation of alternate field-based and remote-sensing methods. *Remote Sens.* **2012**, *4*, 456-483,
676 doi:10.3390/rs4020456.

677 45. Stambaugh, M. C.; Hammer, L. D.; Godfrey, R. Performance of burn-severity metrics and classification
678 in oak woodlands and grasslands. *Remote Sens.* **2015**, *7*, 10501-10522, doi:10.3390/rs70810501.

679 46. Turner, M. G.; Hargrove, W. W.; Gardner, R. H.; Romme, W. H. Effects of Fire on Landscape
680 Heterogeneity in Yellowstone National Park, Wyoming. *J. Veg. Sci.* **1994**, *5*, 731-742, doi:10.2307/3235886.

681 47. Mitri, G. H.; Gitas, I. Z. Fire type mapping using object-based classification of Ikonos imagery. *Int. J.*
682 *Wildl. Fire* **2006**, *15*, 457-462, doi:10.1071/WF05085.

683 48. Yan, G.; Mas, J. -F.; Maathuis, B. H. P.; Xiangmin, Z.; Van Dijk, P. M. Comparison of pixel-based and
684 object-oriented image classification approaches—a case study in a coal fire area, Wuda, Inner Mongolia,
685 China. *Int. J. Remote Sens.* **2006**, *27*, 4039-4055, doi:10.1080/01431160600702632.

686 49. Dean, a. M.; Smith, G. M. An evaluation of per-parcel land cover mapping using maximum likelihood
687 class probabilities. *Int. J. Remote Sens.* **2003**, *24*, 2905-2920, doi:10.1080/01431160210155910.

688 50. CAM *Repoblación de la Superficie Afectada por el Incendio de 26 de Junio de 2003 en los Montes del C.U.P. Nº*
689 *48, Nº 50 Y Nº 54 de la Comarca X -San Martín de Valdeiglesias*; Madrid, 2005;

690 51. Kolden, C. a.; Weisberg, P. J. Assessing Accuracy of Manually-mapped Wildfire Perimeters In
691 Topographically Dissected Areas. *Fire Ecol.* **2007**, *3*, 22-31, doi:10.4996/fireecology.0301022.

692 52. Finco, M.; Quayle, B.; Zhang, Y.; Lecker, J.; Megown, K. a.; Brewer, C. K. Monitoring Trends and Burn
693 Severity (MTBS): Monitoring wildfire activity for the past quarter century using LANDSAT data. *Mov.*
694 *from Status to Trends For. Invent. Anal. Symp.* **2012**, 222-228.

695 53. Lentile, L. B.; Holden, Z. A.; Smith, A. M. S.; Falkowski, M. J.; Hudak, A. T.; Morgan, P.; Lewis, S. A.;

Gessler, P. E.; Benson, N. C. Remote sensing techniques to assess active fire characteristics and post-fire effects. *Int. J. Wildl. Fire* 2006, *15*, 319-345.

54. Safford, H. D.; Stevens, J. T.; Merriam, K.; Meyer, M. D.; Latimer, A. M. Fuel treatment effectiveness in California yellow pine and mixed conifer forests. *For. Ecol. Manage.* **2012**, *274*, 17-28, doi:10.1016/j.foreco.2012.02.013.

55. Morgan, P.; Keane, R. E.; Dillon, G. K.; Jain, T. B.; Hudak, A. T.; Karau, E. C.; Sikkink, P. G.; Holden, Z. A.; Strand, E. K. Challenges of assessing fire and burn severity using field measures, remote sensing and modelling. *Int. J. Wildl. Fire* **2014**, *23*, 1045-1060, doi:10.1071/WF13058.